

Original Research

Adsorption of Rhodamine-B (RhB) and Regeneration of MCM-41 Mesoporous Silica

Thiago Rodrigo Barbosa Barros [†], Thianne Silva Batista Barbosa [†], Tellys Lins Almeida Barbosa [†], Meiry Gláucia Freire Rodrigues ^{†,*}

Federal University of Campina Grande, Academic Unit of Chemical Engineering, Av. Aprígio Veloso, 882-Bodocongó, Zip code 58109-970, Campina Grande-PB, Brazil; E-Mails:

thiagoidbarbosa@gmail.com; thianne.siilva@gmail.com; tellyslins@hotmail.com;
meiry.freire@eq.ufcg.edu.br

[†] These authors contributed equally to this work.

* **Correspondence:** Meiry Gláucia Freire Rodrigues; E-Mail: meiry.freire@eq.ufcg.edu.br

Academic Editor: Prem Kumar Seelam

Special Issue: [Advances in Porous Catalytic Materials](#)

Catalysis Research

2023, volume 3, issue 1

doi:10.21926/cr.2301010

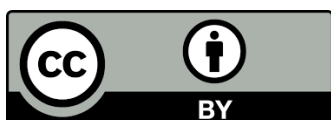
Received: November 01, 2022

Accepted: February 20, 2023

Published: March 01, 2023

Abstract

Rhodamine (RhB) adsorption was carried out on MCM-41 and MCM-41 calcined. The effect of parameters such as pH was investigated. The reusability potential of MCM-41 was also established and the mechanism of RhB adsorption was discussed. MCM-41 was synthesized and calcined, with all samples characterized by X-Ray Diffractometry, X-ray Fluorescence by Dispersive Energy, Infrared Spectroscopy, Scanning Electron Microscopy, and Thermogravimetric analysis. The results of the characterization techniques performed confirmed the formation of the MCM-41 structure. During the adsorption of the RhB dye, high removal percentages and rapid kinetics occur in an acid medium. The adsorption kinetics was evaluated by two models: pseudo-first order and pseudo-second order. The pseudo-first-order kinetic model represented the interaction mechanism well during RhB adsorption by MCM-41. However, the pseudo-second-order model better represented the interaction



© 2023 by the author. This is an open access article distributed under the conditions of the [Creative Commons by Attribution License](#), which permits unrestricted use, distribution, and reproduction in any medium or format, provided the original work is correctly cited.

mechanism during RhB adsorption by MCM-41 calcined. The regeneration study found that the MCM-41 and MCM-41 calcined were maintained at 80 and 90% of their original condition after three successive regeneration cycles. The overall results show that the process could be used as a strategy for environmentally sustainable wastewater treatment.

Keywords

MCM-41; RhB dye; adsorption; kinetics; regeneration

1. Introduction

Pollution from dye effluents has become a serious environmental problem during the last decade, due to the increasing use of dyes in various applications [1]. The worldwide textile industry is the main source of these effluents [2, 3]. Dyes are organic compounds used to color different substrates and are raw materials used in many manufacturing processes, such as: textiles, paper, plastic, leather, food, and pharmaceuticals [4, 5].

RhB is a basic, reddish dye in the Xanthene class, and is highly soluble in water [6]. Xanthene is an organic compound based on a class of dyes; such as fluorescein, eosins, and rhodamines derived from this structure. Xanthene dyes are among the oldest and most used synthetic dyes. Xanthene dyes tend to be fluorescent, giving bright colors, from pinkish yellows to bluish reds [7]. These dyes are similar in color and exist in wastewater effluents; therefore, their removal and determination are important [8]. RhB is widely used as a dye in textiles, food [1, 9], medicine (for animals), and in coloring biological samples [8]. It is also a fluorescent marker for water [6]. The improper disposal of this dye prevents sunlight from penetrating water, leading to serious environmental problems and being toxic and carcinogenic to living beings [10]. Therefore, its removal from aquatic wastewater is essential [11].

The adsorption method has been used in several ways and with different adsorbents to remove the RhB dye from an aqueous solution [1, 12, 13]. Adsorption is one of the superior processes due to its cheapness, ease of operation, high efficiency, and rapidity. The adsorption technique removes organic dyes from aqueous solution by employing efficient materials such as SBA-15, MOFs, MCM-41, etc. [14]. The MCM-41 molecular sieve is a crystalline solid with a highly-defined hexagonal structure, a surface area greater than 700 m²/g, excellent thermal stability, and a structure that can be modified in several ways [15, 16]. These materials have many applications as adsorbents [17-20], especially about the adsorption of dyes [21-25].

The use of the adsorption process as a dye removal technology stands out especially due to the wide variety of adsorbent materials that can be applied. The effective separation of several contaminants by the adsorption process generally requires the porous structure of the adsorbents, which contributes to the improvement of their surface area and adsorption capacity [26].

This study is part of a line of research developed at the New Materials Development Laboratory (LABNOV) at the UFCG. This line of research covered a series of studies on the synthesis and characterization of molecular sieves, which could be used in various processes [27-40]. This work was carried out in two stages, the first stage presented the obtained results on the characterization of both MCM-41 and MCM-41 calcined. The second part investigated the effect of parameters such

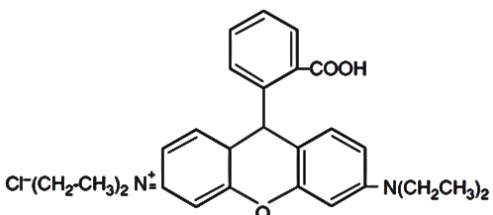
as pH. The adsorption kinetics for RhB using MCM-41 and MCM-41 calcined were also studied. Furthermore, a regeneration study was carried out to investigate the reusability of the adsorbent. To our knowledge, there is no study about the adsorption of the RhB on MCM41.

2. Materials and Methods

2.1 Materials

Cetyltrimethylammonium Bromide (CTAB, 98%), ammonium hydroxide (NH₄OH, 29%) and tetraethylorthosilicate (TEOS, 98%) were purchased from Sigma-Aldrich (MERCK). The main properties of dye RhB are summarized in Table 1.

Table 1 Overview of physicochemical properties of the RhB.

Molecular Formula	Chemical structure	Molecular mass (g/mol)
C ₂₈ H ₃₁ N ₂ O ₃ Cl		479.01

2.2 Synthesis of Silica MCM-41

MCM-41 was prepared using the hydrothermal crystallization method. The proposed method was based on changes made to the procedure reported by the authors [41]. The method was as follows: (A) CTAB was dissolved in deionized water at 50°C under agitation for 30 min. The solution was cooled to approximately 25°C; (B) NH₄OH was added into the solution with stirring for 15 min; (C) Then, the TEOS was introduced; (D) After 2 h, the reaction mixture was submitted to hydrothermal treatment at 30°C for 24 h; (E) The resulting product was filtered, washed with deionized water and then the material was dried at 60°C for 24 h; (F) Material was calcined in a muffle furnace from room temperature up to 550°C, using a 5°C/min heating ramp remaining at the final temperature (550°C) for 7 h.

2.3 Characterization

X-ray diffraction patterns were carried out on a Shimadzu XRD 6000 using Cu K α radiation at 40 kV/30 mA, with a goniometer velocity of 2°/min and step of 0.02° in the 2 θ range from 3.0° to 10.0°.

To obtain the infrared, IR VERTEX 70 equipment from BRUKER was used. The samples in the form of tablets were dried in an oven in advance and placed in the sample holder. The IR spectra were obtained at wavelengths in the 400-4000 cm⁻¹ range with a resolution of 4 cm⁻¹. To identify and quantify the chemical composition of the synthesized samples, an S2 Ranger Bruker dispersive energy X-ray spectrophotometer was used. A VEGA TESCAN scanning electron microscope was used to perform microscopy on the samples. The powder samples were covered with a thin layer of gold by a metallizer and fixed to support with carbon adhesive tape. Thermogravimetric analysis was performed in a Shimadzu DTG-60H Thermal Analyzer in a nitrogen atmosphere with a 50 mL/min

gas flow. The sample was heated from room temperature up to 1000°C, at a heating rate of 10°C/min.

2.4 Batch Adsorption Experiments

2.4.1 Influence of pH

The influence of the pH of the RhB dye solution on the adsorption capacity of each sample was tested with a concentration of 15 mg/L of dye, adjusted to different pH levels. For each sample, 30 mL of dye was used with the mass of each sample being 0.3 g. Samples were prepared with a pH ranging from 1 to 14 in intervals of one unit, totaling 14 samples. The samples were acidified and made alkaline using 3 M hydrochloric acid and 1 M sodium hydroxide solutions. The pH of the dye solution is a parameter of significant influence in determining the adsorption capacity [42].

2.4.2 Adsorption Kinetics

RhB adsorption kinetics were acquired in batch experiments. These experiments were performed at 25°C using a solution of 15 mg/L of RhB, which was put in contact with 0.3 g of samples. Adsorption experiments were conducted in conical flasks at controlled pH (1.0) and under a shaking table at 200 rpm. Aliquots from the solution were collected at time intervals (20 min) between 0 and 180 min. Afterward, the solutions were centrifuged and analyzed for residual dye concentration with a UV-vis spectrophotometer.

The concentration of RhB dye was determined using a UV-VIS 1600 spectrometer with a wavelength of 554 nm [43]. The removal percentage (R%) and the quantity of adsorbed RhB (q) were obtained using Equations 1 and 2, respectively.

$$R\% = \left(\frac{C_i - C}{C_i} \right) * 100 \quad (1)$$

$$q = \frac{V}{m} (C_i - C) \quad (2)$$

where: R% = removal percentage; q = quantity of adsorbed RhB (mg of RhB/g of adsorbent); V = volume of dye solution (L); m = mass of adsorbent (g); C_i = initial concentration of dye solution (mg/L); and C = final concentration remaining after the batch process (mg/L).

2.5 Evaluation of Regenerated MCM-41

The capacity of an adsorbent material to be regenerated and reused is key to its ability to be used in wastewater treatment. To check the ability to reuse MCM-41, repeated runs were performed at the optimum conditions found and adapted by other authors [44]. Each cycle consisted of a 1.0 g sample with 100 mL of dye at pH 1, stirred for 30 min. Regeneration was performed by washing each sample with 100 mL of deionized water and 50 mL of methyl alcohol (MeOH). After washing, the samples were filtered and dried at 60°C for 24 h.

3. Results

3.1 Characterization

Figure 1 shows the diffractogram of MCM-41 obtained from X-ray diffraction. Figure 2 presents the FTIR spectra of MCM-41 and MCM-41 calcined in the range 4000-500 cm^{-1} evaluated at room temperature.

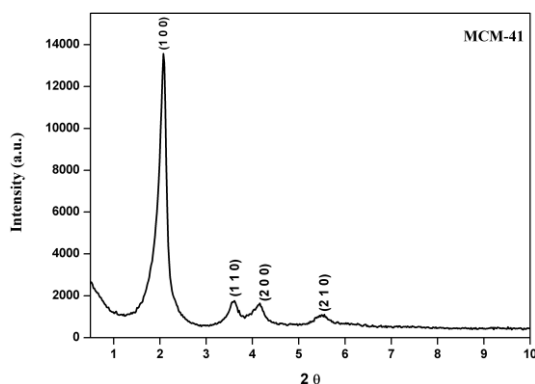


Figure 1 X-ray diffraction patterns of the MCM41.

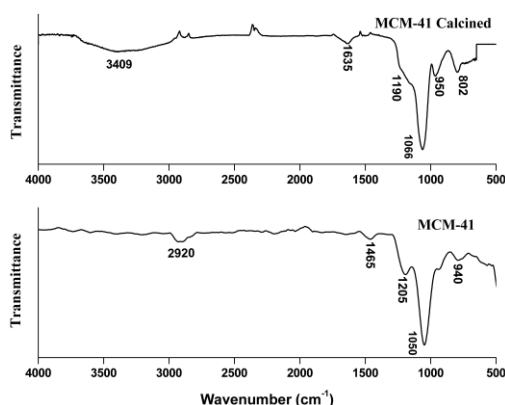


Figure 2 FTIR spectra of the MCM-41 and MCM-41 calcined.

The XRD of the synthesized MCM-41 molecular sieve exhibits an intense peak at $2\theta = 2.2^\circ$ corresponding to the plane (1 0 0) and two to three small peaks between 3.5° and 6.0° due to the planes (1 1 0), (2 0 0) and (2 1 0) that show the presence of ordered mesoporous hexagonal MCM-41 [41, 45-48].

In Figure 2 (MCM-41 and MCM-41 calcined), the spectra show bands in 940 and 950 cm^{-1} corresponding to angular vibrations of the Si-OH bond of the silanol groups existing in the MCM-41 structure. The spectra of the synthesized and calcined samples show bands in the 500-4000 cm^{-1} region characteristic of the fundamental vibrations of the functional groups present in the structures of the molecular sieves MCM-41 [46]. It is possible to observe the presence of a main band at 1050 and 1066 cm^{-1} composed of another secondary band, less developed at 1025 and 1190 cm^{-1} , which corresponds to asymmetric stretches of the Si-O-Si connection [47, 48]. The spectra also show vibrational bands at 1465 and 2920 cm^{-1} attributed to the stretches between CH of the CH_2 and CH_3 groups, which correspond to the presence of the surfactant, cetyltrimethylammonium

bromide (CTAB) which is occluded in the pores of MCM-41 [49]. MCM-41 calcined shows a broadband without definition corresponding to the template's removal.

Chemical composition percentage concentrations determined by Dispersive Energy X-Ray Fluorescence (ED-XRF) for MCM-41 showed a high silicon dioxide (SiO_2) content, 99.85% and some impurities.

Three mass loss events can be observed from the thermogravimetric curve of the synthesized MCM-41 shown in Figure 3. The first event below 150°C related to the desorption of physisorbed water in the pores of the material that corresponds to 4% of mass loss, the second in the range of $150\text{-}320^\circ\text{C}$ attributed to the decomposition of the driving ions (CTAB) where the greater mass loss of 31% and the third between $400\text{-}550^\circ\text{C}$ due to the residual removal of CTAB, resulting from the secondary condensation process of the silanol groups corresponding to 13% of the total loss [48-52].

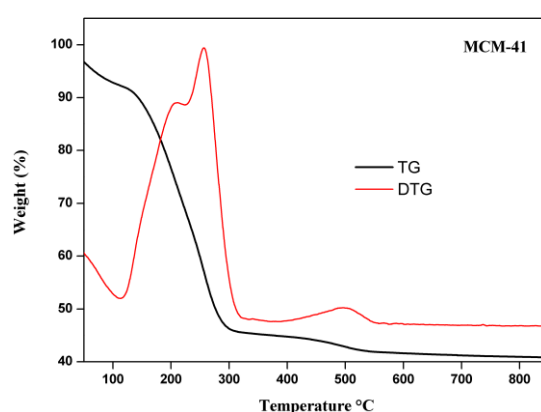


Figure 3 TG/DTG curves of the MCM-41.

The Morphology of MCM-41 (Figure 4) is similar to those of authors [53] who synthesized the MCM-41 using NH_4OH at different temperatures. The particles have spongy, irregular, and non-uniform spherical clusters.

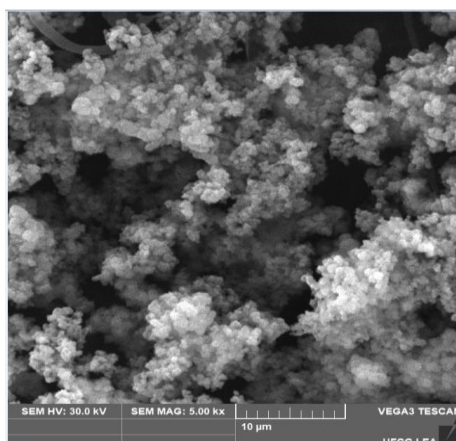


Figure 4 Micrograph of the MCM-41.

Figure 5 (a) shows the adsorption and desorption curves of N_2 for MCM-41 calcined, and (b) shows the pore size distribution obtained through the BJH method.

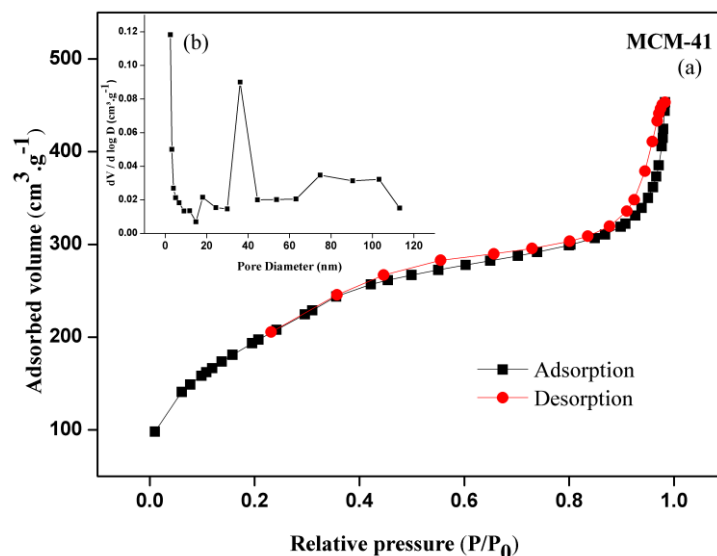


Figure 5 N₂ adsorption and desorption of the MCM-41 calcined isotherm and pore size distributions.

According to the IUPAC classification, the samples exhibited type IV isotherms and different hysteresis loops [54]. According to IUPAC isotherms of this type are typical of mesoporous materials with multilayer adsorption cycles. Nitrogen adsorption occurs on the material surface at a relative pressure (P/P_0) below 0.2. Then the monolayer is formed, and multi-layers develop over it. From (P/P_0) 0.4 there is an increase in the capacity of adsorbed nitrogen, called hysteresis, associated with capillary nitrogen condensation in the mesopores [48]. This behavior is observed for both materials. In the final part of the isotherm, the pore is saturated after capillary condensation. A small amount of N₂ was adsorbed on the outer walls, resulting in a maximum volume of adsorbed gas of approximately 450 cm³/g for MCM-41.

The behavior of the MCM-41 isotherm exhibited H4-type hysteresis that corresponds to porous materials made up of narrow, slit-shaped pores. The pore diameter distribution showed a peak at around 2.70 nm attributed to the micropore region and a peak at 36 nm attributed to the mesoporous region of the MCM-41.

Table 2 shows the values obtained for the network parameter a_0 (nm) which can be calculated in a simplified way using the formula $a_0 = 2d_{100} \cdot (3^{1/2})^{-1}$, where d_{100} corresponds to the interplanar distance in the (1 0 0) diffraction plane. The surface area, S_{BET} (m²/g), was obtained using the BET method and the average pore diameter, D_p (nm), was obtained using the BJH method. V_p (cm³/g) corresponds to the pore volume of the samples and W_t corresponds to the nanometer thickness of the structural wall, calculated as the difference between the network parameter a_0 and the pore diameter, D_p [55, 56].

Table 2 Synthesis parameters and characterization of the MCM-41 calcined.

	S_{BET} (m ² /g)	D_p BJH (nm)	V_p (cm ³ /g)	a_0 (nm)	W_t (nm)
MCM-41	726	3.53	0.64	4.87	1.34

According to Table 2, the BET surface area of MCM-41 calcined is 726 m²/g, a value relative as shown in the literature [57, 58]. The wall thickness of the MCM-41 calcined is by the authors exhibiting a value between 1 and 1.5 nm [16]. This thin wall takes the material to low chemical and hydrothermal stability.

3.2 Batch Adsorption Experiments

3.2.1 Influence of pH

The pH of the aqueous medium is an important factor that can modify RhB adsorption. The chemical characteristics of both adsorbent and adsorbate can vary depending on the pH. The pH of the solution affects the degree of ionization and speciation of various dyes, which subsequently changes the reaction kinetics and equilibrium characteristics of the adsorption process [20, 59]. Experiments were performed to study the influence of the pH on the adsorption capacity of materials, varying the pH from 1 to 13. The experimental results for the RhB adsorption on both samples (MCM-41 and MCM-41 calcined) are shown in Figure 6.

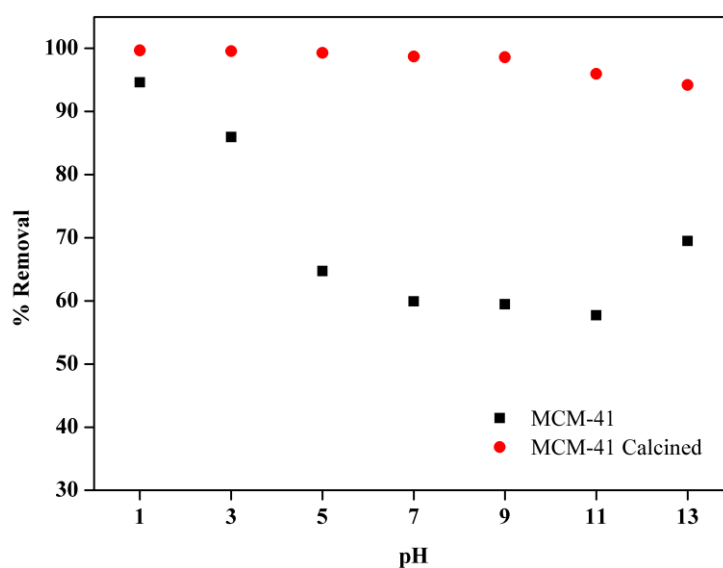


Figure 6 Effect of pH on the adsorption of RhB by MCM-41 and MCM-41 calcined.

For the MCM-41 (Figure 6), the internal pore region is obstructed by the template, meaning that the adsorption of the dye can be effective only on the structure's external surface. MCM-41 showed a low adsorption removal, mainly at pH 7, 9, and 11. It was noted that the most favorable adsorption of RhB dye occurs at acidic pH levels, according to the literature [23, 59, 60].

Results for the MCM-41 calcined (Figure 6) indicate that the effect of pH was not so prominent. As can be seen, the MCM-41 calcined adsorbs and removes high percentages of RhB dye at almost all pH levels, from acidic to basic. This can be attributed to the fact that the adsorption occurred both on the surface of the MCM-41 calcined and in the internal pore region, due to the greater number of active sites on the MCM-41 calcined.

Figure 6 clearly shows that the adsorption of RhB onto the MCM-41 is quite different from the adsorption of the dye onto the MCM-41 calcined.

3.2.2 Dye Adsorption

It must be noted that the surface of the adsorbent changes its polarization according to the pH value of the solution and the isoelectric point (IEP) of the solid [61]. The pH chosen for the tests was lower than the isoelectric point pH_{iep} of MCM-41, which was 1. When the pH of the solution is lower than pH_{iep} , a material surface is positively charged, and the sorption of anionic species to a positively charged sorbent occurs through the Coulomb force of attraction. The opposite occurs at higher pH values [25], when decreasing dye adsorption levels may be attributed to the competition of OH⁻ with the dye ions for the adsorption sites on the material. The increased number of hydroxyl groups decreases the number of positively charged sites and reduces the attraction between the dye and the adsorbent surface [24]. As described in the literature [20], the complex structure of some dyes causes multiple possible interactions among dye molecules and adsorbents.

3.2.3 Adsorption Kinetics

Adsorption kinetics of the RhB dye was determined from batch experiments with constant agitation. Kinetic studies for the adsorption of RhB dye were performed at a 15 mg/L concentration. The pH was adjusted to 1 and 0.3 g of MCM-41 was used in each batch. Figure 7 and Figure 8 show the kinetic curves obtained from the RhB dye adsorption tests for samples (MCM-41 and MCM-41 calcined), that fit the pseudo-first-order and pseudo-second-order models.

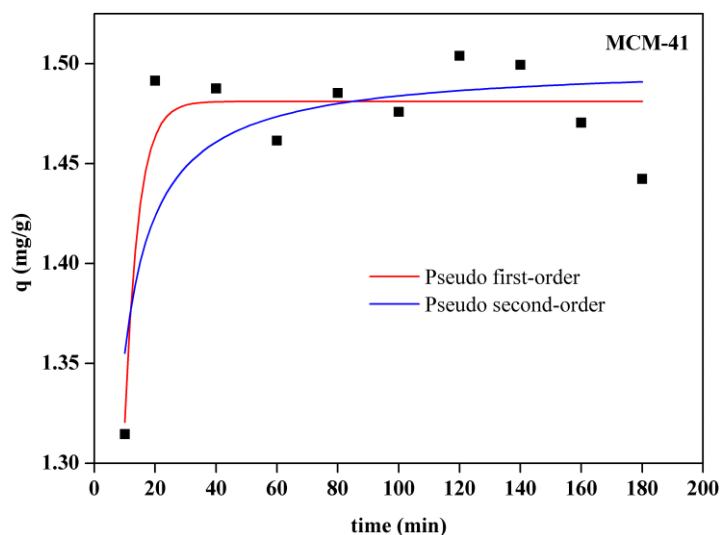


Figure 7 Adsorption kinetics of RhB dye onto MCM-41 and non-linear fits: pseudo-first order and pseudo-second order.

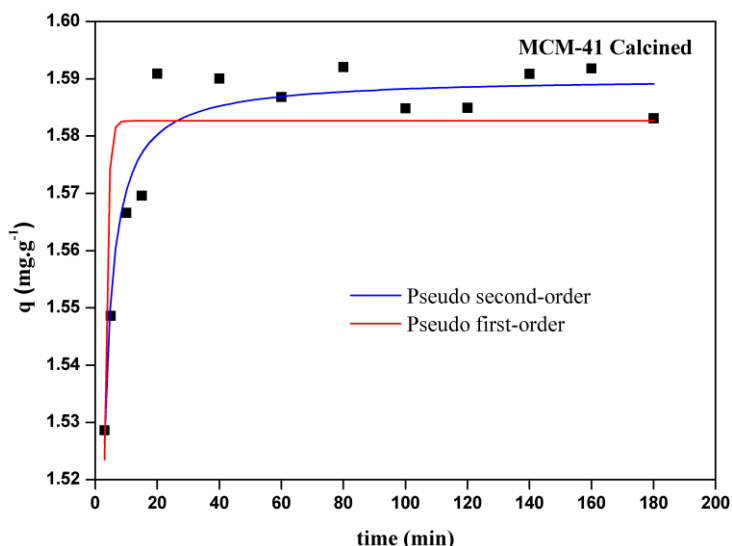


Figure 8 Adsorption kinetics of RhB dye onto MCM-41 calcined and non-linear fits: pseudo-first order and pseudo-second order.

Rapid adsorption was observed in the first 20 minutes of contact time between the RhB dye solution and the material, after which the adsorption equilibrium was established, with few variations in the adsorption capacity until the final contact time of 180 minutes (Figure 7). MCM-41 showed a maximum adsorption capacity of 1.50 (mg/g) in 20 min. The pseudo-first-order was the kinetic adsorption model that best fit the MCM-41 behavior, presenting a good coefficient of determination values. In contrast, the second-order model showed a lower determination coefficient (R^2) due to the low interaction between the chemical species adsorbed on the surface of the adsorbent and the amount adsorbed at steady state [62, 63].

According to the data presented in Figure 8, excellent adsorption was observed for the calcined samples. It is possible to state that, in the first 15 minutes of contact time between the RhB dye solution and the material, the adsorption equilibrium was established, as few variations were seen in the adsorption capacity until the final contact time of 180 minutes. MCM-41 calcined had a maximum adsorption capacity of 1.59 (mg/g) in 80 minutes of contact. kinetic model that best fit, and obtained the best value for the coefficient of determination for the MCM-41 calcined, was the pseudo-second-order model, due to the greater adsorbate-adsorbent interaction characteristic of the **chemisorption** that occurs in this model [64].

Table 3 shows the kinetic parameters of the pseudo-first order and pseudo-second order models obtained from the non-linear model generated by the Origin 8.0® software.

Table 3 Kinetic model parameters for RhB dye adsorption onto MCM-41 and MCM-41 calcined.

Models	Equations	Parameters	
		MCM-41 Calcined	MCM-41
Pseudo-first order	$q = q_{eq} \cdot \exp(-K_1 t)$	$R^2 = 0.691$	$R^2 = 0.847$
		$K = 1.095$	$K = 0.222$
		$q_e = 1.583$	$q_e = 1.481$

Pseudo-second order	$q = \frac{K \cdot q_{eq}^2 \cdot t}{(1 + t \cdot K_2 \cdot q_{eq})}$	$R^2 = 0.926$	$R^2 = 0.578$
		$K = 4.999$	$K = 0.625$
		$q_e = 1.590$	$q_e = 1.500$

3.2.4 Evaluation of Regenerated MCM-41 and MCM-41 Calcined

Reusing the adsorbents (MCM-41 and MCM-41 calcined) was investigated under optimized conditions. Figure 9 shows the data on the removal percentage in each adsorption cycle.

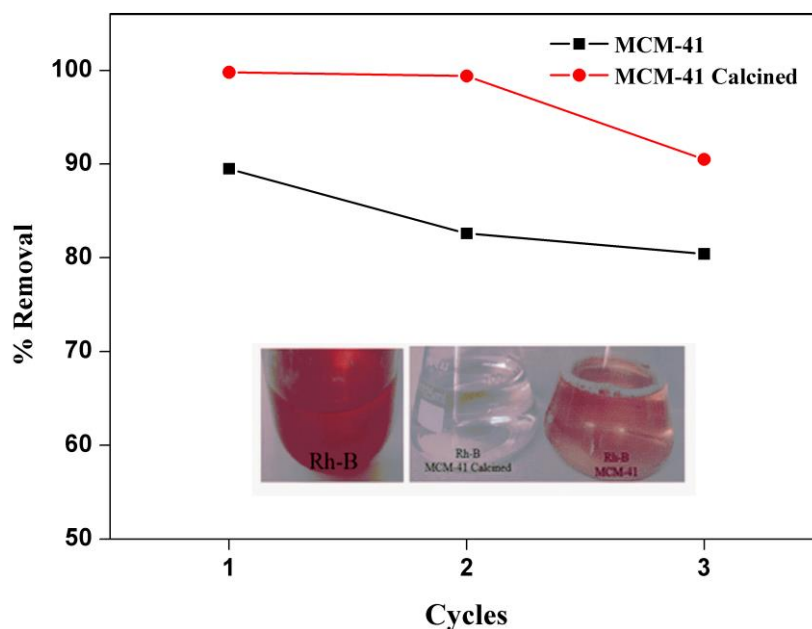


Figure 9 Recyclability tests adsorbed with RhB.

Results in Figure 9, for the reuse of each sample in three consecutive cycles of adsorption of the RhB dye at a pH of 1, showed that the adsorption capacity decreased considerably from the first to the second cycle and from the second to the third cycle, for both samples. MCM-41 calcined had a higher adsorption capacity than the as-synthesized MCM-41, for the three reuse cycles. The molecular structure of RhB (dimension ~ 1.20 nm) [65] compared to the pore diameter (3.5 nm) of the MCM-41 calcined, provides a favorable condition for the entry of this dye molecule into the pores of the adsorbent. Therefore, washing MCM-41 calcined with methanol does not compromise the structure of the mesoporous silica, making this material suitable for reuse up to 3 times after regeneration.

The data obtained in this study on the adsorption capacity of the materials from the adsorption of the RhB dye are shown in Table 4 along with other data from the literature.

Table 4 Various types of adsorbents for the removal of RhB and their maximum adsorption capacity.

Material	Adsorbate dye C ₀ (mg/L)	Regeneration/ N° of cycles	Adsorption capacity (mg/g)	Reference
MCM-41	C ₀ = 15 pH = 1	Methanol/ n = 3	1.56	This work

MCM-41 Calcined	$C_0 = 15$ pH = 1	Methanol/ n = 3	1.74	This work
3A zeolite	$C_0 = 10$ pH = 9	-	0.74	[66]
MCM-22 zeolite	$C_0 = 1.10 \times 10^{-4}$ mol/g	-	1.11	[67]

Reusability experiments were carried out to investigate the performance of the MCM-41. At the end of the adsorption process, the saturated sorbent was separated by filtration, and then regenerated using methanol, followed by drying at 60°C for 24 h. The regenerated adsorbent was reused in a subsequent run under the same conditions.

Based on the adsorption RhB, MCM-41 and MCM-41 calcined were efficient, removing up to 80% of the RhB. The results of adsorption capacity for RhB were 1.35 and 1.52 mg/g for MCM-41 and MCM-41 calcined, respectively.

Lower results were found in the literature [66, 67]. However, it was noted that the MCM-41 and MCM-41 calcined (present study) removed more than the zeolites. Two factors can explain this fact: i) different structures; and ii) different experimental conditions. Compared with the results found in the literature, the MCM-41 and MCM-41 calcined results produced in this study were satisfactory [66, 67].

3.3 Possible Adsorption Mechanisms

The adsorption of RhB dye onto the MCM-41 and MCM-41 calcined was studied to understand the influence of surfactant CTAB on the adsorption behavior. It was observed that several factors significantly influence the adsorption of dyes on mesoporous structures, such as the dye structure itself, the textural and chemical properties of the adsorbent surface, and the specific interaction between the adsorbent surface and the adsorbate [68]. The structure of the MCM-41 consists of SiO₂ tetrahedra ending in siloxane (Si–O–Si) or silanol (Si–OH) groups on the surface [18].

Therefore, it is understood that the adsorption of RhB dye on MCM-41 calcined was higher than that obtained on MCM-41 due to the CTAB chain affecting the adsorption behavior. It was shown that mesoporous materials containing surfactant could limit and restrict the diffusion of molecules within the phase of the materials [69]. Another way to interpret the above results may be with the difference existing in the interactions between basic dyes and surface hydroxyl groups of MCM-41. RhB possesses polar atoms (N), so the interaction between RhB and MCM-41 may be stronger. This may induce a collapse in the pore structure of MCM-41, and then create a sharp decrease in the adsorption capacity. On the other hand, the free silanol groups, after calcination, found on the surface of mesoporous silica, can interact with the nitrogen and hydrogen groups of the dye through hydrogen bonding [70].

After drying, the regenerated samples from the third RhB adsorption cycle were analyzed through FTIR. Figures 10 (a) and (b) show the FTIR spectra in the range 4000-500 cm⁻¹ evaluated at room temperature.

Figure 10 (a) shows the well-known vibration mode of the -CH₂ and -CH₃ groups of the CTAB surfactant of MCM-41 (2935 cm⁻¹). In Figure 10 (a) and (b), the spectra in the range between 3409-1635 cm⁻¹, corresponding to the axial deformation of the C-H bond and the aromatic bonds of RhB [68]. In other bands, at 1190-1205 and 940-950 cm⁻¹, the RhB functional groups are located in the

same regions as those that characterize the groups of MCM-41, indicating a possible interaction of the dye with the silanol groups [71, 72].

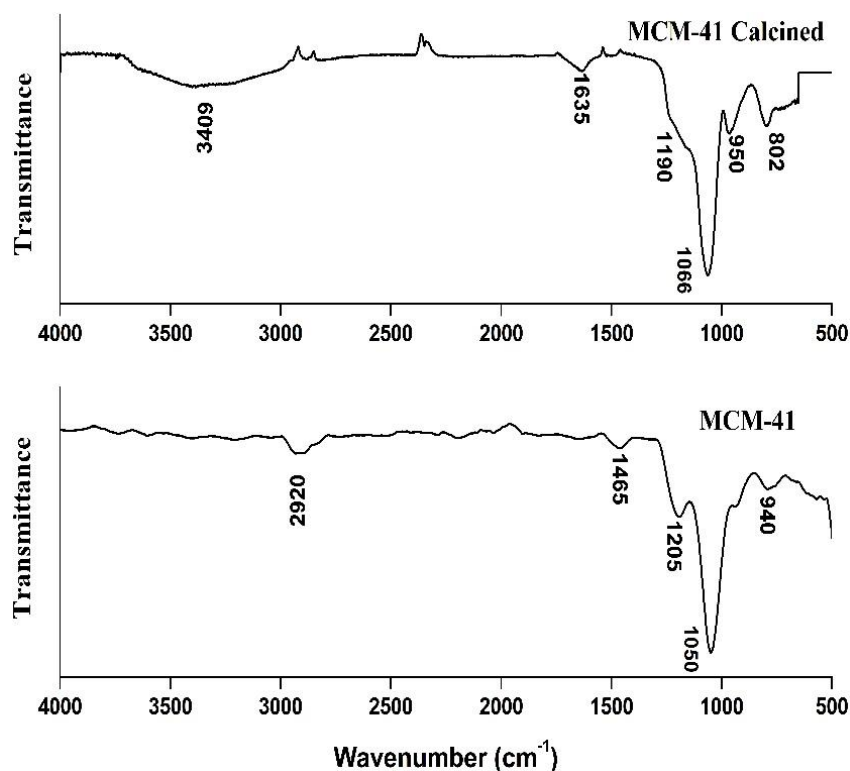


Figure 10 FTIR spectra of the MCM-41 (a) calcined (b) after adsorption of RhB.

4. Conclusions

According to the XRD, ED-XRF, FTIR, and nitrogen adsorption isotherm results, MCM-41 and MCM-41 calcined were effectively synthesized and produced a mesoporous material. This study showed that the MCM-41 and MCM-41 calcined are effective adsorbents for removing RhB dye from an aqueous solution. The results indicate that the template played an important role in adsorption due to its strong hydrophobic properties. The effect of parameters such as pH was studied, finding that acidic conditions favored the RhB dye removal process. MCM-41 showed a greater adsorption capacity at acidic pH levels in all tests performed. Pseudo-first-order and pseudo-second-order kinetic models were fitted to the experimental data. For the MCM-41 system (RhB), The pseudo-first-order model was a bit better for the MCM-41 system (RhB), but for the MCM-41 calcined system (RhB), the pseudo-second-order model fit better. The regeneration of MCM-41 and MCM-41 calcined performed well with RhB after three successive processes. Therefore, MCM-41 and MCM-41 calcined can be used as effective adsorbents for RhB, and also demonstrated favorable regeneration capacity, which is relevant when considering their potential use for industrial sector applications, as well as being an important strategy for environmental sustainability.

Acknowledgments

The authors gratefully acknowledge to the CNPq (Conselho Nacional de Desenvolvimento Científico e Tecnológico) and CAPES (Coordenação de Aperfeiçoamento de Pessoal de Nível Superior) for their financial support.

Author Contributions

Thiago Rodrigo Barbosa Barros: Investigation, Formal analysis, Thianne Silva Batista Barbosa: Investigation, Formal analysis, Writing – Original Draft; Tellys Lins Almeida Barbosa: conceptualization, Formal analysis, Methodology; Meiry Gláucia Freire Rodrigues: Conceptualization, Formal analysis, Funding acquisition, Writing – Review & Editing.

Funding

Coordenação de Aperfeiçoamento de Pessoal de Nível Superior (CAPES).

Competing Interests

The authors have declared that no competing interests exist.

References

1. Bello OS, Alabi EO, Adegoke KA, Adegboyega SA, Inyinbor AA, Dada AO. Rhodamine B dye sequestration using *Gmelina aborea* leaf powder. *Heliyon*. 2020; 6: e02872.
2. Nupearachchi CN, Mahatantila K, Vithanage M. Application of graphene for decontamination of water; implications for sorptive removal. *Groundw Sustain Dev*. 2017; 5: 206-215.
3. Wanyonyi WC, Onyari JM, Shiundu PM. Adsorption of Congo red dye from aqueous solutions using roots of *Eichhornia crassipes*: Kinetic and equilibrium studies. *Energy Procedia*. 2014; 50: 862-869.
4. Hisada M, Tomizawa Y, Kawase Y. Removal kinetics of cationic azo-dye from aqueous solution by poly- γ -glutamic acid biosorbent: Contributions of adsorption and complexation/precipitation to Basic Orange 2 removal. *J Environ Chem Eng*. 2019; 7:103157.
5. Ngulube T, Gumbo JR, Masindi V, Maity A. An update on synthetic dyes adsorption onto clay based minerals: A state-of-art review. *J Environ Manage*. 2017; 191: 35-57.
6. Jain R, Mathur M, Sikarwar S, Mittal A. Removal of the hazardous dye rhodamine B through photocatalytic and adsorption treatments. *J Environ Manage*. 2007; 85: 956-964
7. Wainwright M. Photosensitisers in biomedicine. Chichester: John Wiley & Sons Ltd; 2009.
8. Sharifzade G, Asghari A, Rajabi M. Highly effective adsorption of xanthene dyes (rhodamine B and erythrosine B) from aqueous solutions onto lemon citrus peel active carbon: Characterization, resolving analysis, optimization and mechanistic studies. *RSC Adv*. 2017; 7: 5362-5371.
9. Safitri YA, Indrawan IWA, Winarsih S. Rhodamine B induces oxidative stress and cervical epithelial cell proliferation in the uterus. *Toxicol Rep*. 2015; 2: 1434-1436.

10. Tariq M, Muhammad M, Khan J, Raziq A, Uddin MK, Niaz A, et al. Removal of Rhodamine B dye from aqueous solutions using photo-Fenton processes and novel Ni-Cu@MWCNTs photocatalyst. *J Mol Liq.* 2020; 312: 113399.
11. Asfaram A, Ghaedi M, Hajati S, Goudarzi A, Dil EA. Screening and optimization of highly effective ultrasound-assisted simultaneous adsorption of cationic dyes onto Mn-doped Fe₃O₄-nanoparticle-loaded activated carbon. *Ultrason Sonochem.* 2017; 34: 1-12.
12. Inyinbor AA, Adekola FA, Olatunji GA. Kinetics, isotherms and thermodynamic modeling of liquid phase adsorption of Rhodamine B dye onto *Raphia hookerie* fruit epicarp. *Water Resour Ind.* 2016; 15: 14-27.
13. Dahri MK, Kooh MRR, Lim LB. Remediation of rhodamine B dye from aqueous solution using *Casuarina equisetifolia* cone powder as a low-cost adsorbent. *Adv Phys Chem.* 2016; 2016: 9497378.
14. Sriram G, Bendre A, Altalhi T, Jung HY, Hegde G, Kurkuri M. Surface engineering of silica based materials with Ni-Fe layered double hydroxide for the efficient removal of methyl orange: Isotherms, kinetics, mechanism and high selectivity studies. *Chemosphere.* 2022; 287: 131976.
15. Wang Y, Li L, Liu Y, Ren X, Liang J. Antibacterial mesoporous molecular sieves modified with polymeric N-halamine. *Mater Sci Eng.* 2016; 69: 1075-1080.
16. Meynen V, Cool P, Vansant EF. Verified syntheses of mesoporous materials. *Microporous Mesoporous Mater.* 2009; 125: 170-223.
17. Khan AJ, Song J, Ahmed K, Rahim A, Volpe PLO, Rehman F. Mesoporous silica MCM-41, SBA-15 and derived bridged polysilsesquioxane SBA-PMDA for the selective removal of textile reactive dyes from wastewater. *J Mol Liq.* 2020; 298: 111957.
18. Costa JAS, Jesus RA, Santos DO, Mano JF, Romão LPC, Paranhos CM. Recent progresses in the adsorption of organic, inorganic, and gas compounds by MCM-41-based mesoporous materials. *Microporous Mesoporous Mater.* 2020; 291: 109698.
19. Pei Y, Jiang Z, Yuan L. Facile synthesis of MCM-41/MgO for highly efficient adsorption of organic dye. *Colloids Surf A.* 2019; 581: 123816.
20. Boukoussa B, Hamacha R, Morsli A, Bengueddach A. Adsorption of yellow dye on calcined or uncalcined Al-MCM-41 mesoporous materials. *Arab J Chem.* 2017; 10: S2160-S2169.
21. Rios AG, Matos LC, Manrique YA, Loureiro JM, Mendes A, Ferreira AFP. Adsorption of anionic and cationic dyes into shaped MCM-41. *Adsorption.* 2020; 26: 75-88.
22. Rizzi V, Gubitosa J, Fini P, Nuzzo S, Cosma P. Amino-grafted mesoporous MCM-41 and SBA-15 recyclable adsorbents: Desert-rose-petals-like SBA-15 type as the most efficient to remove azo textile dyes and their mixture from water. *Sustain Mater Technol.* 2020; 26: e00231.
23. Qin P, Yang Y, Zhang X, Niu J, Yang H, Tian S, et al. Highly efficient, rapid, and simultaneous removal of cationic dyes from aqueous solution using monodispersed mesoporous silica nanoparticles as the adsorbent. *Nanomaterials.* 2018; 8: 4.
24. Zhou C, Gao Q, Luo W, Zhou Q, Wang H, Yan C, et al. Preparation, characterization and adsorption evaluation of spherical mesoporous Al-MCM-41 from coal fly ash. *J Taiwan Inst Chem Eng.* 2015; 52: 147-157.
25. Monash P, Pugazhenth G. Investigation of equilibrium and kinetic parameters of methylene blue adsorption onto MCM-41. *Korean J Chem Eng.* 2010; 27: 1184-1191.
26. Bhatnagar A, Minocha AK. Conventional and non-conventional adsorbents for removal of pollutants from water-A review. *Indian J Chem Technol.* 2006; 13: 203-217.

27. Medeiros de Paula G, do Nascimento Rocha de Paula L, Freire Rodrigues MG. Production of MCM-41 and SBA-15 hybrid silicas from industrial waste. *Silicon*. 2020; 14: 439-447.
28. de Paula LN, de Paula GM, Rodrigues MG. Adsorption of reactive blue BF-5G dye on MCM-41 synthesized from chocolate clay. *Cerâmica*. 2020; 66: 269-276.
29. Rodrigues JJ, Fernandes FAN, Rodrigues MGF. The use of cobalt/ruthenium catalyst supported in SBA-15 in the promotion of Fischer-Tropsch synthesis. *Braz J Pet Gas*. 2020; 14: 007-021.
30. Jovelino JR, Rodrigues JJ, Rodrigues MGF. SBA-15 molecular sieve: Synthesis, characterization, and application in oil/water separation. *Braz J Pet Gas*. 2018; 12: 219-227.
31. Rodrigues JJ, Fernandes FAN, Rodrigues MGF. Co/Ru/SBA-15 catalysts synthesized with rice husk ashes as silica source applied in the Fischer-Tropsch synthesis. *Braz J Pet Gas*. 2018; 12: 169-179.
32. da Silva MM, Patrício AC, de Sousa AK, Freire Rodrigues MG, da Silva ML. Synthesis and characterization of MCM-41 by XRD, adsorption capacity and foster swelling tests. *Mater Sci Forum*. 2015; 805: 657-661.
33. Rodrigues JJ, Nogueira ÂC, Rodrigues MGF. Rapid synthesis of mesoporous molecular sieve SBA-15 by different techniques with microwave assistance. *Mater Sci Forum*. 2015; 805: 684-689.
34. Lima LA, Menezes VM, Freire Rodrigues MG. Use residue of bagasse sugar canein synthesis of molecular sieve MCM-41. *Mater Sci Forum*. 2014; 798: 95-99.
35. de Paula GM, Lima LA, Freire Rodrigues MG. SBA-15 Molecular sieve using clay as Silicon sources. *Mater Sci Forum*. 2014; 798: 116-120.
36. Rodrigues JJ, Lima LA, de Paula GM, Freire Rodrigues MG. Synthesis and characterization of molecular sieve SBA-15 and catalysts Co/SBA-15 and Ru/Co/SBA-15. *Mater Sci Forum*. 2014; 798: 100-105.
37. Rodrigues JJ, Fernandes FAN, Rodrigues MGF. Study of Co/SBA-15 catalysts prepared by microwave and conventional heating methods and application in Fischer-Tropsch synthesis. *Appl Catal A*. 2013; 468: 32-37.
38. Rodrigues JJ, Pecchi G, Fernandes FAN, Rodrigues MGF. Ruthenium promotion of Co/SBA-15 catalysts for Fischer-Tropsch synthesis in slurry-phase reactors. *J Nat Gas Chem*. 2012; 21: 722-728.
39. Rodrigues JJ, Lima LA, Lima WS, Rodrigues MGF, Fernandes FAN. Fischer-Tropsch synthesis in slurry-phase reactores using Co/SBA-15 catalysts. *Braz J Pet Gas*. 2011; 5: 149-157.
40. de Sousa BV, Rodrigues MG, Cano LA, Cagnoli MV, Bengoa JF, Marchetti SG, et al. Study of the effect of cobalt content in obtaining olefins and paraffins using the Fischer-Tropsch reaction. *Catal Today*. 2011; 172: 152-157.
41. Cai Q, Lin WY, Xiao FS, Pang WQ, Chen XH, Zou BS. The preparation of highly ordered MCM-41 with extremely low surfactant concentration. *Microporous Mesoporous Mater*. 1999; 32: 1-15.
42. Gómez JM, Galán J, Rodríguez A, Walker GM. Dye adsorption onto mesoporous materials: pH influence, kinetics and equilibrium in buffered and saline media. *J Environ Manage*. 2014; 146: 355-361.
43. Zhang J, Yan X, Hu X, Feng R, Zhou M. Direct carbonization of Zn/Co zeolitic imidazolate frameworks for efficient adsorption of Rhodamine B. *Chem Eng J*. 2018; 347: 640-647.
44. Alardhi SM, Alrubaye JM, Albayati TM. Adsorption of methyl green dye onto MCM-41: Equilibrium, kinetics and thermodynamic studies. *Desalination Water Treat*. 2020; 179: 323-331.

45. Beck JS, Vartuli JC, Roth WJ, Leonowicz ME, Kresge CT, Schmitt KD, et al. A new family of mesoporous molecular sieves prepared with liquid crystal templates. *J Am Chem Soc.* 1992; 114: 10834-10843.
46. Lu D, Xu S, Qiu W, Sun Y, Liu X, Yang J, et al. Adsorption and desorption behaviors of antibiotic ciprofloxacin on functionalized spherical MCM-41 for water treatment. *J Clean Prod.* 2020; 264: 121644.
47. Chen W, Bao Y, Li X, Huang J, Xie J, Li L. Role of SiF groups in enhancing interfacial reaction of Fe-MCM-41 for pollutant removal with ozone. *J Hazard Mater.* 2020; 393: 122387.
48. Bezerra DM, Zapelini IW, Franke KN, Ribeiro ME, Cardoso D. Investigation of the structural order and stability of mesoporous silicas under a humid atmosphere. *Mater Charact.* 2019; 154: 103-115.
49. Koh CA, Nooney R, Tahir S. Characterisation and catalytic properties of MCM-41 and Pd/MCM-41 materials. *Catal Lett.* 1997; 47: 199-205.
50. Gu G, Ong PP, Chu C. Thermal stability of mesoporous silica molecular sieve. *J Phys Chem Solids.* 1999; 60: 943-947.
51. Ng EP, Goh JY, Ling TC, Mukti RR. Eco-friendly synthesis for MCM-41 nanoporous materials using the non-reacted reagents in mother liquor. *Nanoscale Res Lett.* 2013; 8: 1-18.
52. Brahmi L, Ali-Dahmane T, Hamacha R, Hacini S. Catalytic Performance of Al-MCM-41 catalyst for the allylation of aromatic aldehydes with allyltrimethylsilane: Comparison with $TiCl_4$ as lewis acid. *J Mol Catal A.* 2016; 423: 31-40.
53. Grün M, Unger KK, Matsumoto A, Tsutsumi K. Novel pathways for the preparation of mesoporous MCM-41 materials: Control of porosity and morphology. *Microporous Mesoporous Mater.* 1999; 27: 207-216.
54. Sing KSW. Reporting physisorption data for gas/solid systems with special reference to the determination of surface area and porosity. IUPAC commission on colloid and surface chemistry including catalysis. *Pure Appl Chem.* 1985; 57: 603-619.
55. Lin YW, Cheng TW, Lo KW, Chen CY, Lin KL. Synthesis and characterization of a mesoporous Al-MCM-41 molecular sieve material and its moisture regulation performance in water molecule adsorption/desorption. *Microporous Mesoporous Mater.* 2021; 310: 110643.
56. Schwank AJ, Melo DMA, Silva AO, Pergher SBC. Use of rice husk ash as only source of silica in the formation of mesoporous materials. *Cerâmica.* 2013; 59: 181-185.
57. Janus R, Wądrzyk M, Lewandowski M, Natkański P, Łątka P, Kuśtrowski P. Understanding porous structure of SBA-15 upon pseudomorphic transformation into MCM-41: Non-direct investigation by carbon replication. *J Ind Eng Chem.* 2020; 92: 131-144.
58. Kruk M, Jaroniec M, Sayari A. Adsorption study of surface and structural properties of MCM-41 materials of different pore sizes. *J Phys Chem B.* 1997; 101: 583-589.
59. Rahdar S, Rahdar A, Zafar MN, Shafqat SS, Ahmadi S. Synthesis and characterization of MgO supported Fe-Co-Mn nanoparticles with exceptionally high adsorption capacity for Rhodamine B dye. *J Mater Res Technol.* 2019; 8: 3800-3810.
60. Kaur H, Kaur R. Removal of Rhodamine-B dye from aqueous solution onto Pigeon Dropping: Adsorption, kinetic, equilibrium and thermodynamic studies. *J Mater Environ Sci.* 2014; 5: 1830-1838.
61. Weber Jr WJ, Morris JC. Kinetics of adsorption on carbon from solution. *J Sanit Eng Div.* 1963; 89: 31-59.

62. Arlene BSN, Suzamar MCR, Edson N, Aldo JGZ, Patricio PZ. Photocatalytic degradation of dye using nanocomposite TiO₂/oxide of graphen. *Quim Nova*. 2016; 39: 686-690. doi: 10.5935/0100-4042.20160080.
63. Ho YS, Mckay G. Pseudo-second order model for sorption processes. *Process Biochem*. 1999; 34: 451-465.
64. Fan X, Wang W, Li W, Zhou J, Wang B, Zheng J, et al. Highly porous ZIF-8 nanocrystals prepared by a surfactant mediated method in aqueous solution with enhanced adsorption kinetics. *ACS Appl Mater Interfaces*. 2014; 6: 14994-14999.
65. Arica TA, Ayas E, Arica MY. Magnetic MCM-41 silica particles grafted with poly (glycidylmethacrylate) brush: Modification and application for removal of direct dyes. *Microporous Mesoporous Mater*. 2017; 243: 164-175.
66. Rahmani M, Kaykhaii M, Sasani M. Application of Taguchi L16 design method for comparative study of ability of 3A zeolite in removal of Rhodamine B and Malachite green from environmental water samples. *Spectrochim Acta A*. 2018; 188: 164-169.
67. Wang S, Li H, Xu L. Application of zeolite MCM-22 for basic dye removal from wastewater. *J Colloid Interface Sci*. 2006; 295: 71-78.
68. Lafi R, Montasser I, Hafiane A. Adsorption of congo red dye from aqueous solutions by prepared activated carbon with oxygen-containing functional groups and its regeneration. *Adsorp Sci Technol*. 2019; 37: 160-181.
69. Zhou Y, Tao YF, Yang J, Lin WG, Wan MM, Wang Y, et al. Novel phenol capturer derived from the as-synthesized MCM-41. *J Hazard Mater*. 2011; 190: 87-93.
70. Shu Y, Shao Y, Wei X, Wang X, Sun Q, Zhang Q, et al. Synthesis and characterization of Ni-MCM-41 for methyl blue adsorption. *Microporous Mesoporous Mater*. 2015; 214: 88-94.
71. Dias JA, Arantes VL, Ramos AS, Giraldi TR, Minucci MZ, Maestrelli SC. Characterization and photocatalytic evaluation of ZnO–Co₃O₄ particles obtained by high energy milling. Part II: Photocatalytic properties. *Ceram Int*. 2016; 42: 3485-3490.
72. Souza FHM, Leme VFC, Costa GOB, Castro KC, Giraldi TR, Andrade GSS. Biosorption of Rhodamine B using a low-cost biosorbent prepared from inactivated *Aspergillus oryzae* cells: Kinetic, equilibrium and thermodynamic studies. *Water Air Soil Pollut*. 2020; 231: 242.